Properties of model atomic free-standing thin films

Zane Shi,[1] Pablo G. Debenedetti,[2,a)] and Frank H. Stillinger[3]
[1]*Department of Physics, Princeton University, Princeton, New Jersey 08544, USA*
[2]*Department of Chemical and Biological Engineering, Princeton University, Princeton, New Jersey 08544, USA*
[3]*Department of Chemistry, Princeton University, Princeton, New Jersey 08544, USA*

(Received 29 January 2011; accepted 23 February 2011; published online 21 March 2011)

We present a computational study of the thermodynamic, dynamic, and structural properties of free-standing thin films, investigated via molecular dynamics simulation of a glass-forming binary Lennard-Jones mixture. An energy landscape analysis is also performed to study glassy states. At equilibrium, species segregation occurs, with the smaller minority component preferentially excluded from the surface. The film's interior density and interface width depend solely on temperature and not the initialization density. The atoms at the surface of the film have a higher lateral diffusivity when compared to the interior. The average difference between the equilibrium and inherent structure energies assigned to individual particles, as a function of the distance from the center of the film, increases near the surface. A minimum of this difference occurs in the region just under the liquid–vapor interface. This suggests that the surface atoms are able to sample the underlying energy landscape more effectively than those in the interior, and we suggest a possible relationship of this observation to the recently reported formation of stable glasses by vapor phase deposition. © *2011 American Institute of Physics*. [doi:10.1063/1.3565480]

I. INTRODUCTION

The effect of interfaces on the structure, dynamics, and thermodynamics of materials, including supercooled liquids and glasses, is a subject of considerable technical and scientific interest.[1] Important applications of glassy materials, such as organic electronics,[2] nanolithography,[3] corrosion prevention,[4] gas separation,[5] and novel nanocomposites[6–8] involve geometries such as supported, free standing, or confined films, and filler–bulk interfaces, with characteristic dimensions in the 1–100 nm scale. The rational design of these materials and devices requires knowledge of properties such as glass transition temperature,[9,10] physical aging,[11] and gas permeation,[12] and their underlying basis in the microscopic structure and dynamics of the spatially heterogeneous nanoconfined material.

Numerous studies have probed experimentally the interfacial and confinement-induced properties of glass-forming systems (e.g., Refs. 9 and 13–23). This remains a very active area of investigation,[24] in part because of the interest generated by unresolved differences between the various measurements (e.g., Refs. 25–28). A noteworthy recent development is the discovery by Ediger and co-workers that glass films with exceptional kinetic and thermodynamic stability can be formed by vapor deposition.[29–35] Enhanced mobility at the free surface has been invoked as a key mechanism in the formation of such stable glasses.[29] Following Ediger and co-workers' discovery, stable thin film glasses of toluene and ethylbenzene have also been formed by vapor deposition.[36–38]

From a theoretical perspective,[39] the presence of interfaces, hence of imposed spatial heterogeneity, renders one of the major problems in contemporary condensed matter physics, namely the glass transition, even richer and more challenging. Although some computational studies have addressed the effects of confinement and interfaces on the structure, dynamics, and thermodynamics of nonpolymeric systems,[40–45] the majority of investigations to date has focused on confined polymers (e.g., Refs. 46–58). Recently, a schematic facilitated kinetic Ising model representing a thin film, its substrate, and a vapor phase, was shown to reproduce key experimentally observed characteristics of vapor-deposited glasses, including surface-enhanced relaxation kinetics, and the existence of an optimum substrate temperature for stable glass formation.[59]

Motivated by the problem's inherent scientific interest, by the variety of intriguing experimental observations, in particular the recent findings of Ediger and co-workers on stable glass formation, and by the interesting theoretical predictions on the nature of the glassy surface,[39] we have undertaken a systematic computational investigation of the effects of interfaces and geometric confinement on the structure, dynamics, and thermodynamics of glass-forming systems. In this first paper we report our results on the simplest system, a free-standing thin film of an atomic glass-forming mixture.[60] In Sec. II we describe our system and the numerical techniques employed in this investigation. Results on the film's structure, layer-by-layer dynamics, and energetics, including, importantly, an analysis of minimum-energy configurations (inherent structures),[61–64] are presented in Sec. III. The major conclusions as well as suggestions for future work are the subject of the concluding Sec. IV.

a)Author to whom correspondence should be addressed. Electronic mail: pdebene@princeton.edu.

 © 2011 American Institute of Physics

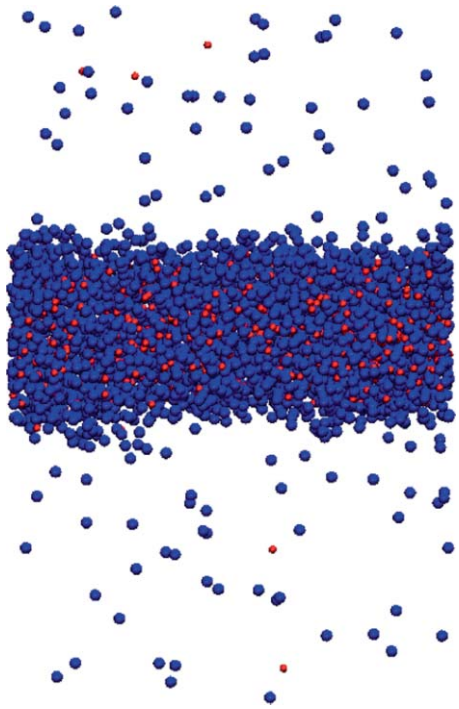

FIG. 1. Snapshot of 4050 atoms in a 22.4 × 22.4 × 35.8 simulation box at $T = 0.7$. The simulation box is stretched in the z direction so that the resulting film does not self-interact. A particles are shown in blue and B particles in red.

II. METHODS

We study the well-known binary Lennard-Jones glass-forming mixture as parameterized by Kob and Andersen,[60] namely, a mixture of 80%A particles and 20%B particles, with parameters $\epsilon_{AA} = 1.0$, $\epsilon_{BB} = 0.5$, $\epsilon_{AB} = 1.5$, $\sigma_{AA} = 1.0$, $\sigma_{BB} = 0.88$, and $\sigma_{AB} = 0.8$. Both types of particles have the same mass, m, and interact via a Lennard-Jones potential $U_{\alpha\beta}(r) = 4\epsilon_{\alpha\beta}[(\sigma_{\alpha\beta}/r)^{12} - (\sigma_{\alpha\beta}/r)^{6}]$. Throughout this paper, all quantities are expressed in reduced units: length in units of σ_{AA}, temperature in units of ϵ_{AA}/k_B, where k_B is Boltzmann's constant and time in units of $(\sigma_{AA}m/\epsilon_{AA})^{1/2}$.

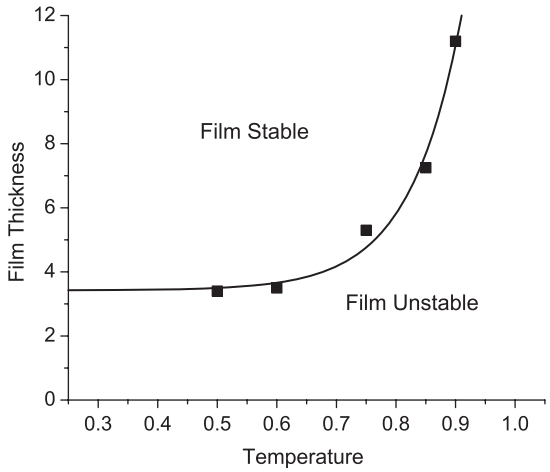

FIG. 2. Temperature and thickness ranges for stable and unstable film formations. The line is a guide to the eye.

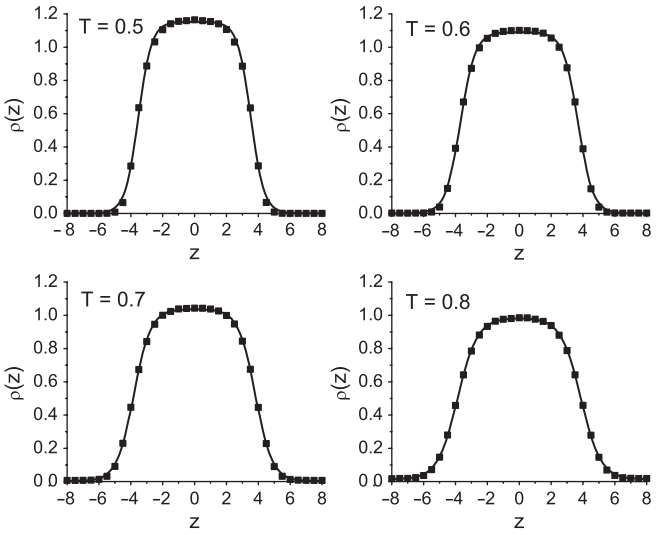

FIG. 3. Density profiles (both species included) for films of 4050 atoms equilibrated at various temperatures. The hyperbolic tangent fit lines give four defining properties of the density profile: the liquid density ρ_L, the vapor density ρ_V, the location of the center of the interface z_e, and the width of the interface d. The values of ρ_L and d are given in Table I, as a function of temperature.

In order to ensure continuity of the potential and its first two derivatives at the potential cutoff (continuity needed for energy minimization calculations), we apply a shifted force correction whereby the force between any two particles, $F_s(r)$, is given by

$$F_s(r) = \begin{cases} F(r) & r < r_1 \\ F(r) + S(r) & r_1 \le r < r_c \\ 0 & r_c \le r. \end{cases} \quad (1)$$

Here, $F(r) = -\partial U_{\alpha\beta}(r)/\partial r$ is the unshifted force, and $S(r)$ is a third order polynomial that is switched on between r_1 and r_c, subject to the constraints $S(r_1) = 0$, $S'(r_1) = 0$, $S(r_c) = -F(r_c)$, $S'(r_c) = -F'(r_c)$. Thus, $F_s(r)$ and its first

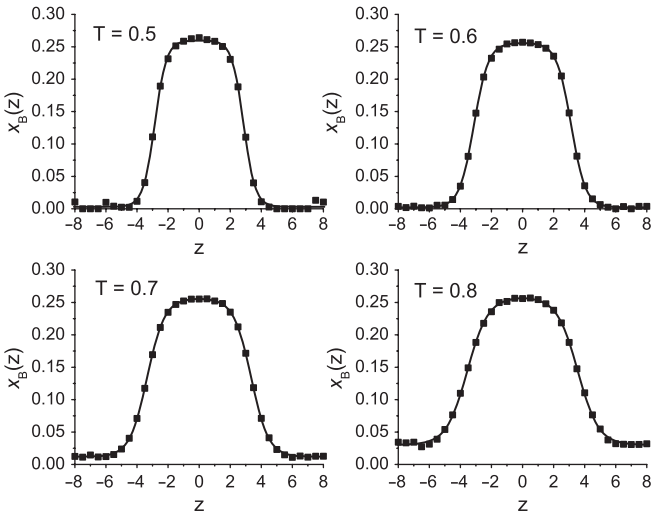

FIG. 4. Mole fraction of B atoms as a function of film depth z for films at various temperatures. Hyperbolic tangent fit lines similar to the form given by Eq. (2) are also shown. Species segregation is evident, with a higher concentration of B atoms in the interior of the film.

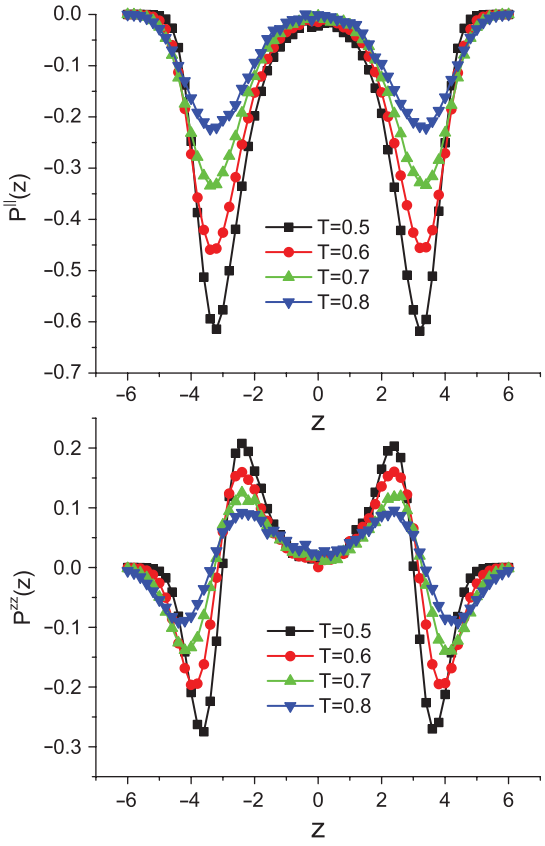

FIG. 5. The lateral (top) and normal (bottom) stress profiles plotted as a function of film depth z for films of various temperatures. Here, positive values correspond to compression and negative values to tension.

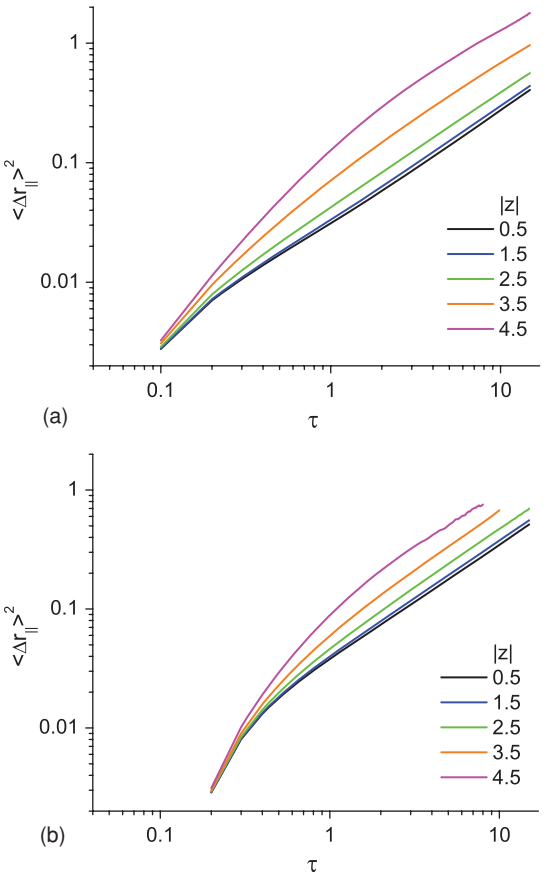

FIG. 6. The lateral mean squared displacement for A (top) and B (bottom) particles, plotted for various layers in a film of 4050 atoms equilibrated at $T = 0.7$.

derivative are smooth and continuous everywhere, and vanish at and beyond r_c. For this study, we set $r_1 = 2.0\sigma_{\alpha\beta}$ and $r_c = 2.5\sigma_{\alpha\beta}$ for all interactions.

To simulate a film, we use a computational cell with periodic boundary conditions that is stretched in the z direction. The dimensions of the box are $L_x = L_y = 22.407$, $L_z = 35.8512$. We initialize the system by placing $N = 4050$ atoms in an fcc lattice of density 1.2 spanning the xy plane and centered in the z direction. The identity of a particle is selected at random while maintaining the overall 4 : 1 ratio of A to B particles. The simulation length along the z-axis is chosen to be large enough such that the film does not interact with its periodic images in the z direction (Fig. 1). The velocity Verlet algorithm of numerical integration is applied, and the molecular dynamics time step used is 0.002. The film is allowed to equilibrate for 2×10^5 time steps, and a coordinate snapshot is taken every 5000 time steps thereafter. The entire simulation is run at fixed particle number, total volume, and temperature (N, V, T), with a Nose–Hoover thermostat.[65] Our results indicate that some properties of the free-standing film, such as the interior density at equilibrium, do not depend strongly on the initialization density and depend only on the temperature T. The maximum temperature that we can simulate before a significant portion of the particles evaporate from the film is $T = 0.9$. In addition, for any given temperature, there exists a minimum thickness, below which the system fails to form a film (Fig. 2). We note that the fit line in Fig. 2 is only a guide to help choose initialization parameters. The precise conditions under which a film is allowed to form are beyond the scope of this paper (the reader is directed to Ref. 66 for a comprehensive study on this topic). Here, we simply choose initialization parameters well inside the existence region to ensure that the film maintains its integrity throughout the simulation.

Naturally, some of the atoms will leave the film and form a vapor phase in the course of the simulation. As a convenient criterion for differentiating the vapor and liquid phases, we say that an atom i belongs to the film if $u_i < -1$, where $u_i = 1/2\Sigma_j U_{\alpha\beta}(r_{ij})$ is the potential energy attributed to an atom, i.e., for every pair interaction between two atoms, half of the potential energy is assigned to one atom and half to the other. We note that this $u_i < -1$ "in film" definition is simply a convenient criterion to identify particles in the film. Indeed, no visually obvious vapor particles have been observed to obey the "in film" criterion. Since the atoms of the film are only a subset of the total atoms in the simulation box, the center of mass of the film is allowed to shift in the z direction. The magnitude of this shift is on the order of σ_{AA}, and this shift must be subtracted during analysis so that the location of the $z = 0$ plane coincides with the film's center of mass.

Finally, we apply the Fletcher and Reeves[67] method of conjugate gradients to perform energy minimization on each coordinate snapshot to study the underlying inherent structures embedded in the film's multidimensional energy

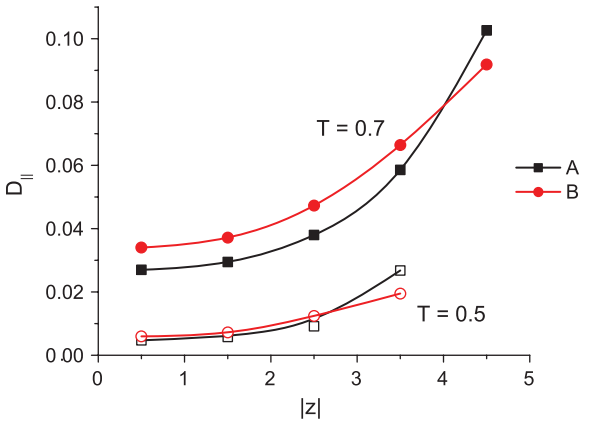

FIG. 7. Lateral diffusion coefficients for films of 4050 atoms equilibrated at $T = 0.5$ and $T = 0.7$. The diffusion rate at the surface is roughly three times that of the interior.

landscape. The particles in the system are moved iteratively along the gradient of the potential energy landscape until $U(\mathbf{r}^N)$, the potential energy as a function of the system's $3N$ translational degrees of freedom, is at a local minimum. The criterion for convergence is satisfied when successive iterations reduce the energy per particle by less than 10^{-7}.

III. RESULTS AND DISCUSSION

A. Film profile

After equilibration, the interior density of a film is dependent only on temperature and not on the initial density. This is due to the nature of the free-standing film, which is free to expand and contract in the normal direction. The density profile at a given temperature is calculated by partitioning the film into slices of thickness $0.5\sigma_{AA}$ from the center of the film and then dividing the average number of particles in each slice by the volume of the given slice (Fig. 3). We perform the following hyperbolic tangent fit[68] to the interfaces of the film:

$$\rho(z) = \frac{1}{2}(\rho_L + \rho_V) - \frac{1}{2}(\rho_L - \rho_V)\tanh\left(\frac{2(|z| - z_e)}{d}\right), \tag{2}$$

where ρ_L is the interior density of the liquid phase, ρ_V is the density of the vapor phase, z_e is the location where the density is the average of ρ_V and ρ_L, and d is a measure of the thickness of the interface. Thus, the fitting parameters give, in principle, important properties of the film. However, the fitted vapor density is invariably vanishingly small, and z_e depends on the number of particles used in the simulation. Accordingly, in Table I we report the values of the two physically relevant, temperature-dependent fitting parameters, ρ_L and d.

TABLE I. Fitted values of the interior density, ρ_L, and interface thickness, d, for free-standing films of various temperatures, T.

T	0.5	0.6	0.7	0.8
ρ_L	1.15	1.09	1.04	0.98
d	0.82	0.94	1.07	1.25

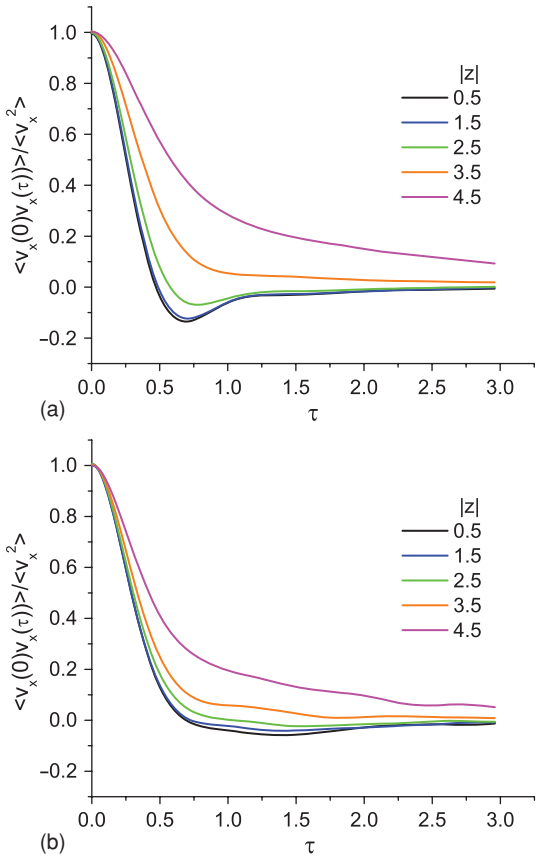

FIG. 8. Normalized velocity autocorrelation function (VACF) for A (top) and B (bottom) particles plotted for various layers in a film of 4050 atoms equilibrated at $T = 0.7$. For both types of particles, the motion near the surface differs from that in the interior of the film. In the interior, the VACF clearly becomes negative, indicating that the atoms on average rebound in the opposite direction after a short time. However, at the surface, the VACF decays monotonically to zero, indicating that, on average, the atoms on the surface do not experience this rebound. This behavior is qualitatively the same at all other temperatures examined.

As shown, with decreasing T, the interior density increases while the thickness of the interface decreases. This is consistent with the simulation results of a pure component Lennard-Jones film as described by Rowlinson and Widom.[68]

Another important property is the distribution of the A and B particles as a function of film depth (Fig. 4). B atoms tend to concentrate toward the center of the film. Since A–A interactions are not as energetically favorable as A–B interactions, the surface is enriched in A atoms. In this way, the system minimizes the energetic cost of forming an interface, namely the loss of half the nearest-neighbor interactions for each surface atom. The corresponding segregation of B atoms toward the center preserves the energetically favored A–B interactions. As a consequence, the vapor phase is dominated by A atoms.

B. Stress

Due to the film's inhomogeneous geometry, the stress varies along the z direction. We consider the pressure normal and parallel to the xy plane, $P^{\perp} = P_{zz}$ and $P^{\parallel} = (P_{xx} + P_{yy})/2$, respectively, and use the virial expression[69] to

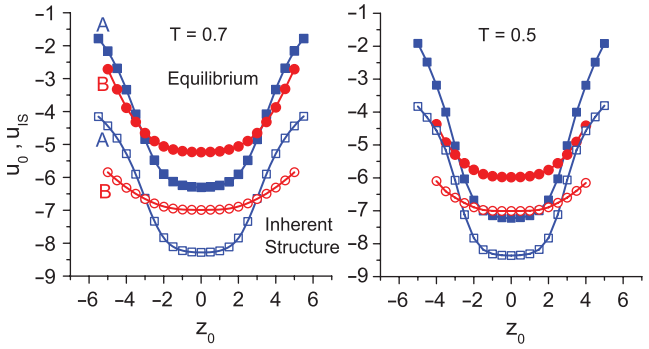

FIG. 9. Average atomic equilibrium and inherent structure potential energy assigned to an atom, as a function of the initial position before minimization, z_0, for atoms of type A and type B. The potential energy assigned to an atom is calculated by splitting pair interaction energies equally between both participating particles.

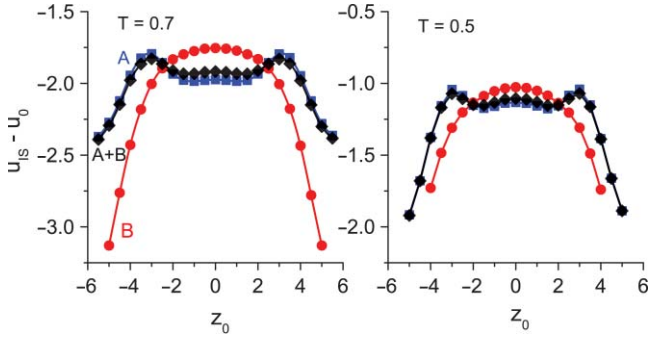

FIG. 10. Average difference of the energy of an atom with respect to its corresponding inherent structure energy, as a function of the initial position before minimization, z_0, for atoms of type A and B. It can be seen that atoms initially at the surface descend deeper down their portion of the energy landscape upon energy minimization.

compute the three diagonal components of the stress tensor in slices of thickness $\Delta z = 0.5\sigma_{AA}$. Figure 5 shows the lateral and normal stress profiles for various simulated temperatures. The lateral stress near the center of the film is small, but appreciable tensile lateral stresses develop in a subsurface region of thickness $\sim 4\sigma_{AA}$, beginning at a depth of $\sim \sigma_{AA}$ beneath the film's surface. The film's subsurface region is also under tensile normal stress, but appreciable normal compression develops in a region of thickness $\sim 2\sigma_{AA}$ located approximately σ_{AA} away from the center. It can also be seen that the film's center is under slight normal compression, and that the magnitude of all stresses increases upon lowering the temperature. This indicates that the predominant contribution to the film's mechanical properties is configurational.

C. Diffusion

Because of the film geometry, particle motion is anisotropic and must be analyzed in the normal and lateral directions. In this study, we are primarily concerned with the lateral diffusion rate. The trajectory of the system was recorded for 5×10^6 time steps, with new time origins t_0 chosen every 500 time steps, to provide independent "experiments" over which to average. To calculate the lateral diffusion coefficient, we partition the film into slices of thickness σ_{AA} starting from the center of the film and use the following modified Einstein diffusion equation:

$$D_{||} = \frac{1}{4} \lim_{\tau \to \infty} \frac{d}{d\tau} \langle \Delta r_{||}(\tau)^2 \rangle_{\text{slice}}, \tag{3}$$

where $D_{||}$ is the lateral diffusion coefficient, and $\langle \Delta r_{||}(\tau)^2 \rangle_{\text{slice}}$ is the average mean squared displacement of the particles that remain in the slice for the entire interval duration τ. For slices that are contained in the interior of the film, the diffusion coefficient is determined by calculating the slope of $\langle \Delta r_{||}(\tau)^2 \rangle$ on the interval $\tau \in [2, 12]$. For slices at the interface, $\langle \Delta r_{||}(\tau)^2 \rangle$ does not become clearly linear until $\tau > 6$, and the slope is calculated on the interval $\tau \in [7, 12]$.

Figure 6 shows the layer-by-layer lateral diffusion of both type A and type B particles for a film at temperature $T = 0.7$. We see that the lateral diffusion coefficient at the surface is roughly three times greater than at the center of the film (Fig. 7). Further insight can be gained by considering a related quantity, the velocity autocorrelation function (Fig. 8). A striking difference between the dynamics of the atoms at the surface as compared to the interior is evident. In the interior, after a short time, the atoms on average "rebound" in the opposite direction. Atoms at the surface, on the other hand, on average do not experience this rebound. As a check of consistency, we also find that both the diffusion coefficient and the velocity autocorrelation function at the center of the film match essentially exactly the corresponding quantities computed for a bulk system with the interior film density and composition as parameters.

D. Inherent structures

We perform an energy minimization[67] on each coordinate snapshot to study the underlying inherent structures (potential energy landscape) (Ref. 61) of these films. Here, we will denote by z_0 the z coordinate of a particle before minimization. Figure 9 shows the average energy per particle before minimization, u_0, and the corresponding inherent structure quantity, u_{IS}, both plotted against z_0. We also plot the difference $u_{IS} - u_0$ as a function of z_0 (Fig. 10). At the film interface, the quantity $|u_{IS} - u_0|$ is much larger than in the interior. In other words, on average, the particles at the surface of the film descend more deeply down their portion of the energy landscape than particles in the film's interior. This is in agreement with theoretical predictions[39] and with the interpretation of the molecular mechanisms underlying the enhanced stability of slow-grown vapor-deposited glasses.[29,30] It suggests that particles at the surface are able to explore the energy landscape more efficiently and point to the pronounced basin anharmonicity introduced by the presence of free surfaces; if the system was harmonic, $u_0 - u_{IS}$ would equal $3/2k_BT$, independent of z.

The difference $|u_{IS} - u_0|$ is also a measure of how far energetically an atom is from its underlying single-particle inherent structure energy. This can be interpreted as a measure of stability, i.e., a region of lower $|u_{IS} - u_0|$ is more stable, in the sense that its energy differs by a comparatively smaller amount from that corresponding to the mechanically

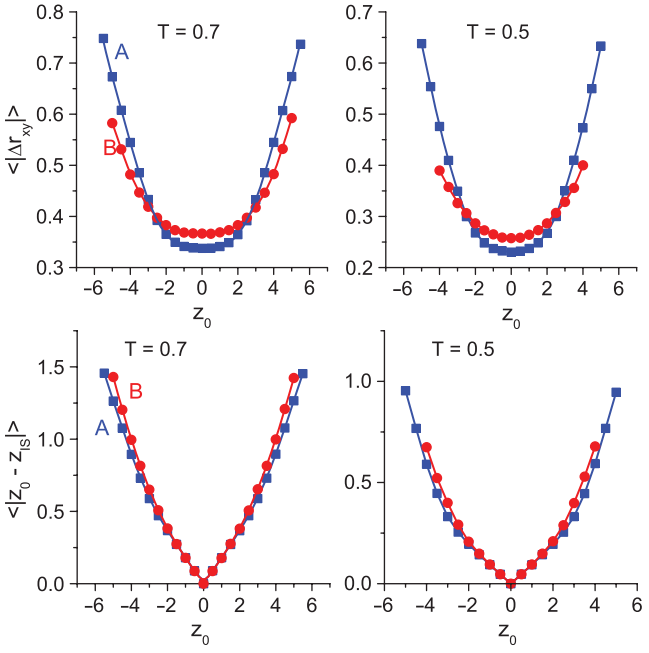

FIG. 11. The average lateral and normal displacements that an atom undergoes during energy minimization as a function of its initial position z_0. It can be seen that atoms near the surface suffer larger lateral and normal displacements upon energy minimization than their counterparts located in the film's interior.

stable state (inherent structure). We see that as we move away from the center, $|u_{IS} - u_0|$ does not increase monotonically, and the region slightly under the interface, where the absolute difference attains a minimum, is then the most energetically stable region of the film. This nonmonotonic behavior is observed at all temperatures examined.

We also plot the average displacement of atoms upon descending down the energy landscape toward the closest local minimum. Figure 11 shows the average lateral and normal displacements as a function of z_0. In both directions, the average physical distance to the inherent structure minimum increases as we move outward from the center of the film. This result, combined with the increased diffusion rate at the surface, shows the more efficient landscape sampling at the free surface.

IV. CONCLUSIONS

In this work we have investigated the properties of an atomic free-standing film. This study is part of an ongoing project aimed at exploring computationally the effects of free surfaces, solid substrates, and spatial inhomogeneity on the structure, dynamics, and thermodynamics of glass-forming systems. The 80%(A)–20%(B) binary Lennard-Jones glass-forming mixture considered here exhibits substantial compositional inhomogeneity, with weaker A–A interactions favored at the free surface and stronger A–B contacts favored inside the film. This preferential enrichment of surface and bulk in A and B, respectively, reflects primarily the energetics of free surface stabilization. Over the range of temperatures explored herein, we observe a substantial enhancement of lateral mobility at the surface with respect to the film's interior. In agreement with theoretical predictions,[39] particles residing at the free surface are able to descend deeper down the energy landscape than particles in the film's interior. Since the difference between equilibrium and inherent structure energy should be independent of position for a harmonic system, this behavior is an indication of the strong basin anharmonicity introduced by the free surfaces.

Our observations suggest several avenues for future inquiry. The possible relevance of our two key observations (enhanced diffusion at the surface, deeper descent down the energy landscape for surface particles) to the recent discovery by Ediger and co-workers of stable glasses formed by slow vapor deposition[29–35] remains to be established. In light of recent reports of surface anisotropy in vapor-deposited stable glasses,[70] simulation of model molecular systems that are capable in principle of adopting different orientations at the surface and in the bulk would be informative. The substrate temperature was shown by Ediger *et al.*[30] to be an important variable for controlling the stability of vapor-deposited glasses. The corresponding computational studies remain to be done. Also of interest would be an investigation of the relative importance of surface mobility and anharmonicity in causing surface particles to descend deeper down the energy landscape. Finally, we have described surface particles as being able to sample the energy landscape more efficiently and providing a general quantitative definition of this idea would be useful. These are some of the aspects of glassy behavior in thin films that we plan to investigate and on which we plan to report in future publications.

ACKNOWLEDGMENTS

P.G.D. gratefully acknowledges the support of the Princeton Center for Complex Materials (National Science Foundation Materials Research Science and Engineering Center Grant No. DMR-0819860) and of the National Science Foundation (Grant No. CHE-0908265).

[1] M. Alcoutlabi and G. B. McKenna, J. Phys. Condens. Matter **17**, R461 (2005).
[2] C. Y. Kwong, A. B. Djurisic, V. A. L. Roy, P. T. Lai, and W. K. Chan, Thin Solid Films **458**, 281 (2004).
[3] S. O. Kim, H. H. Solak, M. P. Stoykovich, N. J. Ferrier, J. J. de Pablo, and P. F. Nealey, Nature (London) **424**, 411 (2003).
[4] A. N. Khramov, N. N. Voevodin, V. N. Balbyshev, and M. S. Donley, Thin Solid Films **447-448**, 549 (2004).
[5] Y. Huang and D. R. Paul, Polymer **45**, 8377 (2004).
[6] M. Mu, A. M. Walker, J. M. Torkelson, and K. I. Winey, Polymer **49**, 1332 (2008).
[7] J. M. Kropka, V. Pryamitsyn, and V. Ganesan, Phys. Rev. Lett. **101**, 075702 (2008).
[8] A. Bansal, H. Yang, C. Li, K. Cho, B. C. Benicewicz, S. K. Kumar, and L. S. Schadler, Nature Mater. **4**, 693 (2005).
[9] R. D. Priestley, C. J. Ellison, L. J. Broadbelt, and J. M. Torkelson, Science **309**, 456 (2005).
[10] C. J. Ellison and J. M. Torkelson, Nature Mater. **2**, 695 (2003).
[11] R. D. Priestley, Soft Matter **5**, 919 (2009).
[12] J. Matthiesen, R. S. Smith, and B. D. Kay, Phys. Rev. Lett. **103**, 245902 (2009).
[13] Z. Fakhraai and J. A. Forrest, Phys. Rev. Lett. **95**, 025701 (2005).
[14] Z. Fakhraai and J. A. Forrest, Science **319**, 600 (2008).
[15] D. Qi, Z. Fakhraai, and J. A. Forrest, Phys. Rev. Lett. **101**, 096101 (2008).
[16] B. M. Besancon, C. L. Soles, and P. F. Green, Phys. Rev. Lett. **97**, 057801 (2006).

[17]H. Bodiguel and C. Fretigny, Phys. Rev. Lett. **97**, 266105 (2006).
[18]W. Zheng and S. L. Simon, J. Chem. Phys. **127**, 194501 (2007).
[19]M. K. Mukhopadhyay, X. Jiao, L. B. Lurio, Z. Jiang, J. Stark, M. Sprung, S. Narayanan, A. R. Sandy, and S. K. Sinha, Phys. Rev. Lett. **101**, 115501 (2008).
[20]A. Serghei, M. Tress, and F. Kremer, J. Chem. Phys. **131**, 154904 (2009).
[21]T. Koga, C. Li, M. K. Endoh, J. Koo, M. Rafailovich, S. Narayanan, D. R. Lee, L. B. Lurio, and S. K. Sinha, Phys. Rev. Lett. **104**, 066101 (2010).
[22]S. Xu, P. A. O'Connell, and G. B. McKenna, J. Chem. Phys. **132**, 184902 (2010).
[23]A. K. Kandar, R. Bhattacharya, and J. K. Basu, J. Chem. Phys. **133**, 071102 (2010).
[24]M. Sikorski, C. Gutt, Y. Chushkin, M. Lippmann, and H. Franz, Phys. Rev. Lett. **105**, 215701 (2010).
[25]Z. Yang, Y. Fujii, F. K. Lee, C. H. Lam, and O. K. C. Tsui, Science **328**, 1676 (2010).
[26]O. K. C. Tsui, in *Polymer Thin Films*, edited by O. K. C. Tsui and T. P. Russell (World Scientific, Singapore, 2008), pp. 267–294.
[27]Z. Jiang, H. Kim, X. Jiao, H. Lee, Y.-J. Lee, Y. Byun, S. Song, D. Eom, C. Li, M. H. Rafailovich, L. B. Lurio, and S. K. Sinha, Phys. Rev. Lett. **98**, 227801 (2007).
[28]Y. Chushkin, C. Caronna, and A. Madsen, Europhys. Lett. **83**, 36001 (2008).
[29]S. F. Swallen, K. L. Kearns, M. K. Mapes, Y. S. Kim, R. J. McMahon, M. D. Ediger, T. Wu, L. Yu, and S. Satija, Science **315**, 353 (2007).
[30]K. L. Kearns, S. F. Swallen, M. D. Ediger, T. Wu, and L. Yu, J. Chem. Phys. **127**, 154702 (2007).
[31]K. L. Kearns, S. F. Swallen, M. D. Ediger, T. Wu, Y. Sun, and L. Yu, J. Phys. Chem. B **112**, 4934 (2008).
[32]K. J. Dawson, K. L. Kearns, M. D. Ediger, M. J. Sacchetti, and G. D. Zografi, J. Phys. Chem. B **113**, 2422 (2009).
[33]K. J. Dawson, K. L. Kearns, L. Yu, W. Steffen, and M. D. Ediger, Proc. Natl. Acad. Sci. U.S.A. **106**, 15165 (2009).
[34]K. L. Kearns, M. D. Ediger, H. Huth, and C. Schick, J. Phys. Chem. Lett. **1**, 388 (2010).
[35]K. L. Kearns, T. Still, G. Fytas, and M. D. Ediger, Adv. Mater. **22**, 39 (2010).
[36]E. León-Gutierrez, G. Garcia, M. Clavaguera-Mora, and J. Rodríguez-Viejo, Thermochim. Acta **492**, 51 (2009).
[37]E. León-Gutierrez, G. Garcia, A. F. Lopeandia, M. T. Clavaguera-Mora, and J. Rodríguez-Viejo, J. Phys. Chem. Lett. **1**, 341 (2010).
[38]E. León-Gutierrez, A. Sepúlveda, G. Garcia, M. Clavaguera-Mora, and J. Rodríguez-Viejo, Phys. Chem. Chem. Phys. **12**, 14693 (2010).
[39]J. D. Stevenson and P. G. Wolynes, J. Chem. Phys. **129**, 234514 (2008).
[40]T. M. Truskett and V. Ganesan, J. Chem. Phys. **119**, 1897 (2003).
[41]J. Mittal, J. R. Errington, and T. M. Truskett, Phys. Rev. Lett. **96**, 177804 (2006).
[42]J. Ghosh and R. Faller, J. Chem. Phys. **125**, 044506 (2006).
[43]J. Ghosh and R. Faller, J. Chem. Phys. **128**, 124509 (2008).
[44]F. Calvo and D. J. Wales, J. Chem. Phys. **131**, 34504 (2009).
[45]T. G. Lombardo, N. Giovambattista, and P. G. Debenedetti, Faraday Discuss. **141**, 359 (2008).
[46]K. Binder, A. Milchev, and J. Baschnagel, Annu. Rev. Mater. Sci. **26**, 107 (1996).
[47]C. Mischler, J. Baschnagel, and K. Binder, Adv. Colloid Interface Sci. **94**, 197 (2001).
[48]F. Varnik, J. Baschnagel, and K. Binder, Phys. Rev. E **65**, 021507 (2002).
[49]Q. Wang, Q. Yan, P. F. Nealey, and J. J. de Pablo, J. Chem. Phys. **112**, 450 (2000).
[50]J. A. Torres, P. F. Nealey, and J. J. de Pablo, Phys. Rev. Lett. **85**, 3221 (2000).
[51]D. S. Fryer, R. D. Peters, E. J. Kim, J. E. Tomaszewski, J. J. de Pablo, P. F. Nealey, C. C. White, and W. L. Wu, Macromolecules **34**, 5627 (2001).
[52]R. S. Tate, D. S. Fryer, S. Pasqualini, M. F. Montague, J. J. de Pablo, and P. F. Nealey, J. Chem. Phys. **115**, 9982 (2001).
[53]T. S. Jain and J. J. de Pablo, Macromolecules **35**, 2167 (2002).
[54]T. S. Jain and J. J. de Pablo, Phys. Rev. Lett. **92**, 155505 (2004).
[55]K. Yoshimoto, T. S. Jain, P. F. Nealey, and J. J. de Pablo, J. Chem. Phys. **122**, 144712 (2005).
[56]R. A. Riggleman, K. Yoshimoto, J. F. Douglas, and J. J. de Pablo, Phys. Rev. Lett. **97**, 045502 (2006).
[57]S. Peter, H. Meyer, and J. Baschnagel, J. Chem. Phys. **131**, 014902 (2009).
[58]S. Peter, H. Meyer, and J. Baschnagel, J. Chem. Phys. **131**, 014903 (2009).
[59]S. Léonard and P. Harrowell, J. Chem. Phys. **133**, 244502 (2010).
[60]W. Kob and H. C. Andersen, Phys. Rev. E **51**, 4626 (1995).
[61]F. H. Stillinger and T. A. Weber, Phys. Rev. A **25**, 978 (1982).
[62]F. H. Stillinger and T. A. Weber, Science **225**, 983 (1984).
[63]F. H. Stillinger, Science **267**, 1935 (1995).
[64]F. H. Stillinger, Phys. Rev. E **59**, 48 (1999).
[65]W. G. Hoover, Phys. Rev. A **31**, 1695 (1985).
[66]R. Godawat, S. N. Jamadagni, J. R. Errington, and S. Garde, Ind. Eng. Chem. Res. **47**, 3582 (2008).
[67]R. Fletcher and C. M. Reeves, Comput. J. **7**, 149 (1964).
[68]J. S. Rowlinson and B. Widom, *Molecular Theory of Capillarity* (Dover, New York, 2002).
[69]W. Smith, "Calculating the pressure," Collaborative Computational Projects 5(CCP5): http://www.ccp5.ac.uk/ftpfiles/ccp5.newsletters/39/pdf/smith.pdf (1993).
[70]K. J. Dawson, L. Zhu, L. Yu, and M. D. Ediger, J. Phys. Chem. B **115**, 455 (2011).